Molecular machines directly observed by high-speed atomic force microscopy

メタデータ	言語: English
	出版者:
	公開日: 2017-10-03
	キーワード (Ja):
	キーワード (En):
	作成者: Ando, Toshio
	メールアドレス:
	所属:
URL	http://hdl.handle.net/2297/34130

Review

Molecular machines directly observed by high-speed atomic force microscopy

Toshio Ando
Department of Physics, Kanazawa University, Kakuma-machi, Kanazawa 920-1192, Japan

ABSTRACT

Molecular machines made of proteins are highly dynamic and carry out sophisticated biological functions. The direct and dynamic high-resolution visualization of molecular machines in action is considered to be the most straightforward approach to understanding how they function but this has long been infeasible until recently. High-speed atomic force microscopy has recently been realized, making such visualization possible. The captured images of myosin V, F1-ATPase, and bacteriorhodopsin have enabled their dynamic processes and structure dynamics to be revealed in great detail, giving unique and deep insights into their functional mechanisms.

1. Introduction

The vital activities of cells depend on the activities of molecular machines made of proteins with various functions. Various approaches have been taken to examine their functional mechanism. The most frequently taken approach has been the structural analysis of proteins by X-ray crystallography, NMR, and electron microscopy. This is because the function of proteins is closely related to their structure. More than 60,000 proteins have been clarified in terms of the detailed three-dimensional structure. The detailed structure is useful in revealing local interactions between amino acid residues but is often less useful in revealing the global interdomain and interprotein communication which plays an essential role in the operation of molecular machines. Moreover, the obtained structures are limited to static snapshots, while proteins in general and molecular machines in particular are highly dynamic in nature. To access the dynamics of proteins in action, single-molecule fluorescence microscopy [1,2] and optical trap nanometry [3,4] have been developed and used. In single-molecule fluorescence microscopy, individual protein molecules are labeled with fluorophores at a specific locus of the protein and observed under a fluorescence microscope. Although a subset of molecular events can be indirectly revealed for the labeled portion of the molecule, other portions are completely invisible. In optical trap nanometry, mechanical events occurring in a molecule (displacement or force production) are measured by optical detection of the displacement of a microsphere attached to the molecule or its interacting partner. Thus, most, if not all, of the structural information is omitted in these frequently performed measurements.

Simultaneously and directly observing both the structure and dynamics of molecular machines in action is considered to be the most straightforward approach to understanding how they operate. To this end, Ando and colleagues embarked on the development of high-speed atomic force microscopy (HS-AFM) two decades ago. AFM is a unique imaging tool that enables the high-resolution visualization of objects made of any material in any environment (vacuum, air, and liquids) [5]. However, it takes at least 30 s (usually minutes) to capture an image, and therefore, moving objects cannot be imaged or can only be blurrily imaged. Through the creation of new devices and techniques and the improvement of the first version of our instrument [6], HS-AFM has now been realized [7,8] and can capture images every 40–100 ms. Importantly, the function of fragile molecules is not disturbed by the interaction with a cantilever tip. This performance has made it possible to visualize, for example, myosin V walking along an actin filament [9], bacteriorhodopsin responding to light [10,11], and rotorless F_1-ATPae with rotationally propagating conformational changes [12]. Unlike single-molecule fluorescence microscopy, various dynamic events of molecules appear in an AFM movie without their preplanned selection. Therefore, we can observe several facets of molecular action in detail in a single imaging experiment. Moreover, the visualized molecular action that appears on the video can often be interpreted straightforward without intricate analyses and interpretations, enabling convincing conclusions to be reached. These excellent general features of HS-AFM imaging greatly facilitate and accelerate our understanding of the functional mechanisms of molecular machines. However, a drawback of HS-AFM imaging is that the sample preparation for HS-AFM imaging is not as easy as that for fluorescence microscopy imaging.

This review first describes the principle of AFM, which is followed by an outline of the HS-AFM instrumentation as well as its speed and low-invasiveness performance. Then, imaging studies carried out by my group on three different molecular machines are presented. Finally, a brief perspective is given on upcoming biological research that will be opened up by high-speed AFM.

2. Principle of AFM

Among a number of operation modes, HS-AFM employs the tapping mode [13]. In this mode, the cantilever is oscillated at its first resonant frequency f_c. A stylus probe attached to the free end of the cantilever is intermittently brought into contact with the sample. The mechanical response of the cantilever upon this contact (change in amplitude) is measured and then the detected amplitude is compared with a preset amplitude value (i.e., set point amplitude). The difference between them (error signal) is input to a proportional-integral-derivative (PID) controller, whose output is sent to a voltage amplifier (piezodriver). The sample stage, which is attached to a piezoactuator-based z-scanner, is finally moved in the z-direction by the piezodriver output so that the error signal approaches zero. (see Fig. 1). This series of

operations is repeated many times at different points of the sample surface during lateral scanning of the sample stage. Consequently, the movement of the sample stage traces the sample surface, and therefore, the feedback controller output at each xy position represents the sample height at that position. Thus, the sample surface topography is constructed from the recorded feedback controller output.

In the tapping mode, the cantilever tip is vertically oscillated. Hardly any lateral force is exerted between the tip and the sample, provided that the lateral displacement of the sample stage is very small (~0.1 nm) for the period of tip-sample contact. As cantilevers are much stiffer in the lateral direction than in the vertical direction, this nearly zero load is advantageous for imaging biological samples. For protein molecules, the resolution is generally 2–3 nm in the lateral direction and 0.1–0.2 nm in the vertical direction, although depending on the sharpness of the tip. AFM imaging relies on sequential height measurement at many different points on the sample surface. Moreover, because AFM contains slow mechanical devices (a cantilever and a scanner), the temporal resolution of conventional AFM is usually on the order of minutes.

3. High-speed AFM

High-speed AFM was realized by the enhancement of the response speed of all the devices contained in the closed feedback loop, particularly of the cantilever and scanner, as well as by passive and active damping of the scanner vibration. Details of the instrumental development are described elsewhere [7]. Here, the speed performance of the major devices employed in our HS-AFM instrument is summarized. The response speed of the cantilever was increased by its size reduction [14,15]. Small cantilevers with a highest response speed are 6 μm long, 2 μm wide, and 90 nm thick (BL-AC7DS-KU3, custom made by Olympus) and have the following mechanical properties: f_c ~ 1.2 MHz in water (~3.5 MHz in air), quality factor Q_c ~ 2 in water, and spring constant k_c ~ 0.2 N/m. Therefore, the time constant $Q_c/(\pi f_c)$ with which the oscillating cantilever responds to tip-sample contact is 0.53 μs. The cantilever oscillation amplitude is detected by a fast detector every half or one cycle of oscillation (detection time, 0.42–0.83 μs) [6,7]. The fastest piezoactuator-based z-scanner, which is displaceable up to ~800 nm at 100 V and controlled by an active damping technique [16], responds within 0.36 μs when driven at 100 kHz. As a result of these shortened response times and the compensation for the time delay by the (P + D) operation of the PID feedback controller, the overall feedback bandwidth f_B has now reached ~110 kHz.

4. Highest possible imaging rate

The feedback bandwidth is defined by the z-scanner displacement (i.e., feedback) frequency f_B at which a phase delay of $\pi/4$ or a time delay of $1/(8f_B)$ occurs when tracing the sample

surface. Because of this delay, the cantilever oscillation amplitude A cannot be exactly maintained at its set point amplitude A_s, which results in a larger tip-tapping force (and $A < A_s$) in uphill regions of the sample and a smaller tip-tapping force (and $A > A_s$) in downhill regions [17,18]. When the tip-tapping force applied to the sample is excessive, the scan velocity V_s in the x-direction has to be reduced so that the phase delay θ becomes smaller than $\pi/4$.

The highest possible imaging rate (i.e, highest possible frame rate) R_{max} depends on the feedback bandwidth f_B as well as on the imaging conditions, the spatial frequency of the corrugation on the sample surface ($1/\lambda$) to be imaged, and the sample fragility. The imaging conditions are given by the scan range in the x-direction W and the number of scan lines N. When the x-scanner is displaced at velocity V_s, the z-scanner is driven at frequency $f = V_s/\lambda$. Thus, the imaging rate is $R = V_s/(2WN) = \lambda f/(2WN)$. When the sample is sufficiently strong for withstanding the excessive tip force due to the $\pi/4$ phase delay, the feedback frequency f can be increased up to f_B. In this case, we obtain $R_{max} = \lambda f_B/(2NW)$. In reality, fragile biological molecules cannot withstand a large tip force. Denoting the maximum phase delay allowable for a fragile molecule as θ_{max}, the highest possible imaging rate is given by $R_{max} = 2\lambda f_B\theta_{max}/(\pi NW)$.

According to our experiences of HS-AFM imaging of protein molecular machines such as F_1-ATPase and myosin V, the maximum possible phase delay is approximately $\pi/9$ for a cantilever free oscillation amplitude of A_0 = 1–2 nm and a set point amplitude of $A_s = 0.9 \times A_0$. For example, for λ = 5 nm, N = 100, and W = 100 nm, R_{max} is 12 fps.

5. Low invasiveness

Under the conditions of A_0 = 1–2 nm, $A_s = 0.9 \times A_0$, and $\theta = \pi/9$, the maximum tapping force is estimated to be about 100 pN for typical proteins with height h_0 ~5 nm when small cantilevers with spring constant k_c = 0.2 N/m are used. This force sounds large because motor proteins generate a force of only a few pN. However, it should be noted that the mechanical quantity that affects the sample (i.e., causes a change in momentum) is not the force itself but the impulsive force (the product of the force acting on the sample and the time during which the force acts). The time during which force acts is short (~100 ns or less) for small cantilevers with a resonant frequency of 1.2 MHz in water. Thus, the magnitude of the impulsive force is small.

The effect of tip tapping on the sample can also be estimated from the energy loss of an oscillating cantilever. When a cantilever with k_c = 0.2 N/m is oscillated at A_0 = 1 nm, its mechanical energy is only ~24 k_BT (similar to the energy of ATP hydrolysis, ~20 k_BT), where k_B is Boltzmann's constant and T is 300 K. Even when all of this energy is lost to excite the sample, the energy will be distributed into many degrees of freedom within the tapped portion of the sample and will quickly dissipate into more degrees of freedom including those of the

surrounding water molecules (see below). In actual imaging experiments, such events of complete energy loss happen only very rarely, if at all, and the cantilever oscillation amplitude is generally maintained at $0.9 \times A_0 = 0.9–1.8$ nm. On average, the energy loss after every tapping is very small: $\frac{1}{2}k_c(A_0^2 - A_s^2)/Q_c = 2.3–9\ k_BT$.

A tip oscillating at a high f_c in water iteratively taps the sample. When an image with an area of $W_x \times W_y$ nm^2 is captured at an imaging rate R, a molecule with a top surface area (A_{top} nm^2) perpendicular to the tip is tapped $f_c/R \times A_{top}/(W_xW_y)$ times per frame. For example, under the conditions (f_c ~1 MHz, R = 12.5 fps, and $W_x \times W_y$ = 45 × 22 nm^2) used for the non-invasive imaging of rotorless F_1-ATPase (i.e., without the γ subunit) [12], one molecule of rotorless F_1-ATPase (A_{top} ~100 nm^2) is tapped ~8,000 times per frame and ~4 million times in total during the 40 s successive imaging. Nonetheless, the rotorless F_1-ATPase is fully functional throughout the imaging, as shown later. This clearly indicates that the energy transferred from the oscillating tip to the sample does not accumulate in the sample but dissipates quickly (much faster than the oscillation period of the cantilever of ~1 μs).

6. HS-AFM imaging of molecular machines

Although only a few years have passed since the establishment of HS-AFM instrumentation in 2008 [7], a number of HS-AFM imaging studies have already been conducted on various protein systems. However, the number of studies that have revealed the structure dynamics of molecular machines in action is limited: myosin V walking on an actin filament [9], rotorless F_1-ATPase with rotationally propagating conformational changes [12], light-driven proton pump bacteriorhodopsin responding to light [10,11], and trimeric $P2X_4$ receptor with a dilating central pore in ATP [19]. Other studies have focused on diffusion processes [20-23], dynamic interactions between molecules [24-28], self-assembly processes [29,30], enzymatic-reaction-coupled molecular processes [18,31-36], and dynamics occurring with DNA origamis [37-39]. In most of these studies, the structure of the molecules involved in the dynamic processes was not well resolved. Nonetheless, important results inaccessible with other approaches have been obtained.

For example, in the observation performed by Igarashi and collaborators on the hydrolysis of cellulose fibers by cellulase [31,32], unidirectional processive movement of the cellulase molecules was demonstrated. Moreover, the retardation of the enzymatic reaction with time, which has been previously observed in biochemical assays, was revealed to arise from traffic congestion of moving molecules [32]. In the observation performed by Scheuring and colleagues on the dynamic association and dissociation between membrane-embedded ATP-synthase c-rings with 6.5 nm diameter [24], their association was revealed to be driven by the “hydrophobic mismatch” [40] between the hydrophobic thickness of the lipid bilayer and the length of the hydrophobic region of the membrane-embedded c-rings. Moreover, from the distribution of the center-to-center distance of a c-ring dimer, the potential energy

distribution was obtained, which showed that an energy minimum of –3.5 k_BT occurred at a center-to-center distance of 10.3 nm (T = 300 K).

Below, imaging studies conducted by my group on the structure dynamics of molecular machines in action are described in detail.

6.1. Walking myosin V

Double-headed myosin V (M5), which functions as a cargo transporter in cells, has been extensively studied (see review [41]). It moves processively along an actin filament [42,43] towards the plus end of the filament in a hand-over-hand manner, advancing 36 nm [44-46] in every ATP hydrolysis cycle [47]. "Hand-over-hand" means that the two heads step alternately, exchanging leading and trailing roles at each step, very much like "walking". In spite of this well-established understanding of how M5 steps, here are still fundamental questions to answer. How is the chemical energy liberated by ATP hydrolysis used to generate the forward movement? How is the powerstroke (lever-arm swing) coupled with the ATPase cycle, if at all? If it really is coupled, which chemical transitions are involved in the generation of tension and lever-arm swing? These fundamental questions have long been explored in muscle contraction studies and a consensus is thought to have already been reached for some of them. Are there any inconsistencies when the consensus view is applied to the motility of M5? Previous single-molecule measurements of M5 stepping do not seem to have answered these questions clearly. Therefore, we performed imaging studies on M5 to demonstrate the power of HS-AFM [9]. Its imaging results were not only consistent with the well-established facts mentioned above but also solved some of the fundamental questions that had previously been difficult to address.

6.1.1. Step motion of myosin V

Partially biotinylated actin filaments were immobilized on a mica-supported phospholipid bilayer surface containing biotin-lipid through streptavidin with a low surface density. The positively charged lipid 1,2-dipalmitoyl-3-trimethylammonium-propane (DPTAP, 5%) was included in this lipid bilayer to facilitate observing the characteristic sideways figure of actin-bound M5-HMM (tail-truncated M5). M5-HMM moving processively with ~36 nm steps was clearly visualized at 7 fps (Fig. 2A). As illustrated in Fig. 2B, the two-headed bound M5-HMM exhibited distinct structural features that are consistent with previous electron microscopy observations [48,49]; the neck–motor domain junction appears smooth in the leading head but is V-shaped in the trailing head without exception, because the neck regions emerge from different parts of the motor domain. The short coiled-coil tail was mostly tilted towards the minus end of actin. These features can be used to determine the polarity of actin when the bound M5-HMM is stationary. When DPTAP was absent in the lipid bilayer, the average translocation velocity was similar to that measured by fluorescence microscopy under the same buffer solution condition, indicating no effect of the tip–sample interaction on the

motor activity. However, we could not observe the molecular behavior during a step in detail as it was completed within a frame. To slow down the step, more streptavidin molecules were placed on the substrate surface as moderate obstacles to the advance. This method allowed the visualization of the stepping process (Figs. 2C, D).

After trailing head detachment, the leading head appeared to spontaneously rotate from the reverse arrowhead orientation towards the arrowhead orientation (the term "arrowhead" originates from the configuration of single-headed myosin bound to an actin filament in the rigor state). Before completing this rotation, the leading head was briefly halted by colliding with a streptavidin molecule in its natural path. In this halted state, the detached trailing head was at its furthest from the actin filament (thus, the two heads were aligned nearly straight, pointing in opposite directions) and slightly rotated around the neck-neck junction (second frame in Fig. 2C). Then, the leading head overcame the streptavidin blockade and rotated to take the arrowhead orientation. Accompanied by this further rotation, the trailing head bound to a forward site of the actin filament to become the leading head, completing one step. Here, it was clearly revealed that during and before the completion of a step, the trailing head never interacts with actin and hence passively moves forwards, driven by the rotating leading head. Thus, the "inchworm" mechanism (a molecule moves forward like an inchworm, in which one head always leads while the other head follows) considered for kinesin [50] as well as the "biased diffusion" mechanism (a molecule moves forward by directional diffusion according to the hypothetical potential slope created along the actin helix) proposed for M5 [51] can be ruled out. The rotation of the leading head is the swinging lever-arm motion itself initially proposed by Hugh Huxley for the powerstroke of muscle myosin [52].

6.1.2. Generation of tension

The seemingly spontaneous rotation of the leading head following trailing head detachment suggests that the intramolecular tension required for the advance already existed in the two-headed bound molecule. In this bound state, the trailing head is in the arrowhead orientation which is the natural orientation, at least for the ADP-bound or nucleotide-free head. Hence, the intramolecular tension is not produced by the bound trailing head. On the other hand, the leading head is not in the natural orientation (i.e., reverse arrowhead orientation) and hence pays an energy cost to generate the intramolecular tension. In fact, the bound leading head is slightly curved outwards, while the trailing head is straight. Upon trailing head detachment, the constraint that keeps the bound leading head in the unnatural orientation is removed, and hence the leading head spontaneously rotates forwards, meaning that the bound leading head is in a strained prestroke state and that the lever arm swing is not accompanied by a chemical transition at the leading head. This conclusion was reinforced by the observation that the short coiled-coil tail of two-headed bound M5-HMM sometimes unfolded and then the leading head rotated from the reverse arrowhead orientation to the arrowhead orientation, which was very similar to the swinging lever arm motion observed

during a step. The uncoiling is caused by intramolecular tension, not by the interaction with the oscillating cantilever tip. This is suggested by the fact that some single-headed species are also contained in the sample of M5-HMM purified through actin binding and dissociation [53].

In general, during the actomyosin ATPase cycle, the strained prestroke state has been thought to always be formed through Pi release from an ADP–Pi-bound head weakly interacting with actin [54,55]. Thus, it may be considered that the strained prestroke state, which is formed directly by the binding of the ADP-bound leading head to actin, does not participate in the forward step in ATP. However, we observed molecular behavior in ATP indicating that it does participate in the step. In two-headed bound M5-HMM, both of the motor domains frequently exhibited brief dissociation and reassociation on the same actin filament (or a brief translocation of ~5 nm along the actin filament), whereas M5-HMM remained at approximately the same position on the filament. We have termed this behavior "foot stomp". Foot stomps were more frequently observed at the leading head than at the trailing head. The briefly detached leading head does not carry bound Pi because Pi was released from an ADP–Pi-bound M5 head when it initially bound to actin. This rapid release of Pi is a feature of the actin-activated M5 ATPase reaction [56]. Nevertheless, the detached leading head with only ADP bound rebinds to actin, still in the reverse arrowhead orientation, and then swings forward following trailing head detachment. The detachment of the leading head during a foot stomp is not caused by ATP binding to the leading head. As described in the next section, a nucleotide-free leading head is often sharply bent. However, we never observed a sharply bent leading head before a foot stomp.

6.1.3. Mechanism of hand-over-hand movement

The leading head of two-headed bound M5-HMM is straight (slightly curved outwards) in ADP or ATP, while it is often sharply bent under the nucleotide-free condition. Therefore, simply by looking at the conformation of the leading head, we can judge whether or not the leading head contains nucleotides. To estimate the ADP dissociation rate constant at the leading head, M5-HMM bound to actin at various concentrations of ADP was observed, and then the lifetime of the straight leading head was analyzed as a function of ADP concentration. The ADP dissociation rate constant at the leading head was estimated to be 0.1/s. This means that ADP is released from the leading head every 10 s on average. However, M5-HMM walks many steps in 10 s, meaning that ADP does not dissociate from the leading head. That is, before ADP dissociation from the leading head, the leading head is switched to the trailing head during walking. ADP dissociation, the subsequent ATP binding, and the resulting detachment from actin solely occur at the trailing head. This is the basis underlying the processive hand-over-hand movement. This mechanism was previously inferred from various indirect experiments [47,57-61] but has now been clearly and directly demonstrated by high-speed AFM observation.

6.1.4. Newly raised questions

The swinging lever-arm hypothesis is no longer a hypothesis. HS-AFM visualized its occurrence with irrefutable clarity. However, our HS-AFM observation results raise question on the mechanochemical coupling mechanism which has been modeled in the context of the swinging lever-arm hypothesis for muscle contraction (Fig. 2E). In this model, the structural configurations are considered to be tightly coupled to the nucleotide states of the motor domain. The M–ADP–Pi state (M denotes the myosin head) is considered to play an essential role in head binding to actin. In this state, the head takes a prepowerstroke conformation resulting from the recovery stroke of the neck domain, which facilitates its binding to actin in the reverse arrowhead orientation. Coupled to the dissociation of Pi after binding to actin, the myosin is considered to swing its neck only once from the reverse arrowhead orientation to the arrowhead orientation and finally take the postpowerstroke conformation. Thus, in this model, the myosin head must pass through the chemical state of M–ADP–Pi to generate a force and move forward. However, the observation by HS-AFM of walking M5-HMM shows that the lever-arm swing spontaneously occurs after trailing-head detachment from actin. Moreover, the tension responsible for the lever-arm swing can be generated by the ADP-bound leading head (after foot stomping), without directly passing through an ADP–Pi-bound chemical state. In addition, two-headed bound M5-HMM in ADP can generate sufficient tension to cause the occasional unwinding of the short coiled-coil tail (i.e., force generation occurs spontaneously). Therefore, the recovery stroke or the prepowerstroke conformation, which has been considered to occur uniquely in the ADP–Pi-bound state, does not appear to be necessary for the lever-arm to swing. Thus, the chemical energy liberated by ATP hydrolysis does not appear to be used for the recovery stroke, tension generation and the lever-arm swing. M5 can step forward once the trailing head detaches from actin without any chemical transitions.

We would, however, inevitably encounter a “perpetuum mobile problem” if we supposed that neither tension generation nor lever-arm swing require any energy input. Even in ADP or in the nucleotide-free condition, the foot stomp occurs at both the leading and trailing heads of two-headed bound M5-HMM, with more frequent occurrence at the leading head than at the trailing head [9]. When the trailing head detaches from actin, the molecule takes a forward step by the spontaneous swing of the leading head. On the other hand, when the leading head detaches from actin, the molecule would not take a backward step because the trailing head is bound to actin in a stable orientation (i.e., the arrowhead orientation). Thus, without any energy input, the M5-HMM molecule can be considered to step forward many times (albeit slowly), even with the less frequent occurrence of foot stomps at the trailing head. This is forbidden perpetuum motion. However, in this gedankenexperiment, the flexibility of the neck-motor domain junction or positional fluctuations of the molecule bound to actin via a single head are not considered. Taking these effects into account, we can expect the

occurrence of a backward step after leading head detachment from actin, although its probability is low. Thus, the principle of detailed balance can hold between the forward step after trailing head detachment and the backward step after leading head detachment, resulting in no net movement of M5 when no energy is input. For example, in the presence of 1 mM ADP, the proportion of foot stomp frequency observed at the leading head was about 0.8, while it was 0.2 at the trailing head. This ratio of 4:1 appears to be insufficient for the detailed balance. However, the foot stomps occur very fast compared with the imaging rate used (7 fps) and the bound M5-HMM almost always stays at the same position after foot stomping at the leading head. The observed ratio of 4:1 is therefore likely to be an underestimate.

From numerous X-ray crystallography and electron microscopy studies, there is no doubt that myosin changes its conformation upon binding to nucleotides and takes a prepowerstroke-like conformation in the ADP–Pi-bound state [49,62-67]. As mentioned above, this prepowerstroke-like conformation certainly facilitates the binding of the head (the leading head in the case of M5) to actin in the reverse arrowhead orientation. However, in the conventional view of the mechanochemical coupling of myosin (Fig. 2E), the conformations of myosin have long been considered to be inflexible. This is mainly due to the fact that the static three-dimensional structures of myosin have often been used to construct models for its mechanochemical coupling. In reality, they are flexible. Otherwise, M5 could not bind to an actin filament via both heads under the ADP-bound and nucleotide-free conditions. However, it can do so even in the absence of nucleotides, which is consistent with the results of other studies [48,57]. Thus, myosin takes two (or multiple) conformations even under a given nucleotide condition (or a given biochemical state). Myosin can go back and forth between different conformations but its dynamic equilibrium shifts to one side depending on the nucleotide condition. Our HS-AFM observations of M5-HMM indicated that structural fluctuations indeed exist and enable the myosin head to take the prepowerstroke configuration even in the ADP-bound and nucleotide-free states. In addition, it was also indicated that the degree of fluctuation depends on the nucleotide state since the leading head of M5-HMM was observed to bind to actin most easily in ATP, next in ADP, and then in the absence of nucleotides. Recently, it has also become possible to study the flexible structures of myosin with the use of spectroscopy and site-directed labeling with fluorescent and spin probes (see review [68]). For example, when a spin probe is attached to the regulatory light chain of myosin in muscle fibers, the spin probe angle relative to the fiber axis was observed to be distributed widely around two peaks with nearly equal populations in ATP (in contracting and relaxed fibers), while in the rigor state it was distributed around two peaks with markedly different populations [69].

The flexibility of the myosin head conformation raises the question of whether the chemical energy of ATP hydrolysis is really used to change the conformation. In the conventional view, the myosin head with a strained conformation in the prepowerstroke state must retain energy that is then liberated during powerstroke. However, the prepowerstroke

and postpowerstroke conformations are in dynamic equilibrium without markedly different populations. Therefore, the energy difference between the two conformations is very likely to be less than 3 k_BT (T = 300 K). Thus, we can conclude that although the conformational change of the myosin head caused by the recovery stroke is an effective strategy for facilitating its binding to actin in the reverse arrowhead orientation, the energy required to produce the prepowerstroke conformation is much less than that liberated by ATP hydrolysis.

Let us perform another gedankenexperiment. Each head of M5 is assumed to be labeled with a chromophore. Upon light absorption, the head-bound chromophore is assumed to alter the conformation of the head so that the head dissociates from actin. When a light pulse only illuminates the trailing head of an M5 molecule, the molecule spontaneously steps forward after trailing head detachment. By repeating this directed light illumination only at the trailing head, we can move the molecule for a long distance in one direction.

Therefore, it appears plausible that a large fraction of the chemical energy liberated by ATP hydrolysis is used elsewhere and is likely to be used to detach a nucleotide-free bound myosin head from actin. How much energy is required for this detachment? The unbinding (rupture) force was previously measured to be ~15 pN by AFM [70]. The rupture distance was also estimated to be 1.7–2.5 nm in this study. This rupture distance is unusually long compared with 0.23 nm for an antigen-antibody [71], 0.15–0.3 nm for streptavidin-biotin [72], and 0.05–0.3 nm for α-actinin-actin [73]. This long rupture distance is consistent with the fact that actin-myosin interfaces contain bonds formed between flexible loops [74,75]. From the values of rupture force and rupture distance, the energy required to rupture the actin-myosin rigor bond is 6–9 k_BT, which is 30–45% of the chemical energy of ATP hydrolysis (~20 k_BT). This mechanically estimated value is approximately consistent with the value of 9 k_BT estimated biochemically for the free-energy change in the dissociation A–M → A + M [76], where A denotes actin. For the ATP-induced dissociation A–M + T → A + M–T (T denotes ATP), the free-energy change is biochemically estimated to be ~10 k_BT, which is similar to that for the mechanical dissociation A–M → A + M. However, one may argue as follows against the statement that a large fraction of the chemical energy liberated by ATP hydrolysis is used to detach a nucleotide-free bound myosin head from actin; ATP is not yet hydrolyzed in the actin-myosin dissociation step; thus, the energy of ATP hydrolysis is not yet liberated. However, since the account balance of energy should be considered for the whole cycle of the ATPase reaction, the ATP-binding energy can be used as part of the energy of ATP hydrolysis.

6.2. Rotary catalysis of rotorless F_1-ATPase

The $\alpha_3\beta_3\gamma$ complex, which is the minimum unit of F_1-ATPase and retains the full ATPase activity, is a rotary motor (Fig. 3A) [77-79]. The coiled-coil part of the rotary shaft γ is inserted in the central cavity formed by a stator ring $\alpha_3\beta_3$ where three α and three β subunits are arranged alternately [80]. Three ATP binding sites are located at the α-β interfaces, mainly

in the β subunits. The rotation of γ occurs in the counterclockwise direction as viewed from the exposed globular portion of γ (or from the C-terminal side of $\alpha_3\beta_3$). In the ATPase cycle, three β subunits take different chemical states: ATP-bound, ADP-bound, and nucleotide-free (empty) states [77,80]. Each chemical state cyclically propagates over the three β subunits. Thus, there is strong cooperativity between the three β subunits. How is this cooperativity engendered? There is no direct contact between the β subunits and the β-γ interaction is always different for the three β subunits because γ has no symmetry. Considering these facts, it was proposed that interactions with γ control and determine the conformational and catalytic states of the individual β subunits [81]. This idea was reinforced by studies showing that the backward mechanical rotation of γ with an external force reverses the chemical reaction toward ATP synthesis [82,83], whereas forced forward rotation results in accelerated ATP binding [84]. This view was, however, challenged by the finding that even when γ is shortened so that most γ-β interaction sites are removed, the short γ still rotates unidirectionally [85]. However, using single-molecule optical microscopy, there was no means of observing the rotation after the complete removal of γ. Thus, we exploited the power of HS-AFM to resolve this issue [12].

$\alpha_3\beta_3$ with Lys_7-tags at the N-termini of the β subunits was covalently immobilized on an amino-reactive mica surface. An image of the C-terminal side of $\alpha_3\beta_3$ without nucleotides shows a pseudo sixfold symmetric ring (Fig. 3B). Each subunit has an upwardly protruding portion at the inner top side of the ring but three of these portions at alternate positions are higher. By the comparison of this image with a simulated AFM image (Fig. 3D) constructed from the crystal structure of nucleotide-free $\alpha_3\beta_3$ (PDB code, 1SKY) [86] (Fig. 3C), the three subunits showing higher protrusions were identified as the β subunits. In 1 mM AMP-PNP, the shape of $\alpha_3\beta_3$ became triangular and the central hole became obscure (Fig. 3E). Only one subunit had a higher protrusion together with an outwardly extended distal portion, which was identified to be an empty β by the comparison of the AFM image with a simulated one (Fig. 3G) constructed from the crystal structure of a nucleotide-bound $\alpha_3\beta_3\gamma$ subcomplex (PDB code: 1BMF) [80] from which γ was removed (Fig. 3F). In addition, the two subunits with retracted distal portions were identified to be nucleotide-bound β subunits.

When imaged in 2–4 μM ATP at 12.5 fps, distinct conformational dynamics occurred at the β subunits (Fig. 3H). Each β exhibited a conformational transition between the outwardly extended high state (open (O) state) and the retracted low state (closed (C) state). The following prominent features were observed: (i) only one β assumes the O-state, and (ii) when the O-to-C transition occurs at one β, the opposite C-to-O transition occurs simultaneously at its counterclockwise neighbor β in most cases. Thus, the O conformation propagates counterclockwise (see the highest pixels, each marked with a red circle in Fig. 3H). The ATP hydrolysis rates at 2, 3, and 4 μM ATP were approximately one-third of the rates of conformational propagation at 2, 3, and 4 μM ATP, respectively. Thus, the conformational propagation is tightly coupled with the ATPase reaction. The cumulative rotation angle of the

highest pixel with discrete 120° steps increases linearly with time until the end of imaging (40 s in total). Thus, the function of $\alpha_3\beta_3$ is completely retained throughout the imaging. The $\alpha_3\beta_3$ molecule is tapped with the oscillating tip ~4 million times in total during this successive imaging.

These dynamic transitions indicate that the O-to-C transition occurs when ATP is bound to an empty β, while the C-to-O transition occurs when an ADP-bound β releases ADP. Thus, the empty, ADP-bound, and ATP-bound β subunits are arranged counterclockwise in this order, and therefore, the observed conformational propagation demonstrates rotary catalysis by the $\alpha_3\beta_3$ subcomplex. Thus, we reach the most important conclusion that the intrinsic cooperativity responsible for torque generation to rotate γ is elicited through the β-β interplay alone and γ is passively subjected to torque causing it to rotate [12].

6.3. Bacteriorhodopsin responding to light

A membrane protein, bacteriorhodopsin (bR), is a light-driven proton pump that transfers protons across the membrane from the cytoplasmic side to the extracellular side [87,88]. bR comprises seven transmembrane α-helices (named A–G) surrounding the retinal chromophore covalently bound to Lys216 via a protonated Schiff base [89,90]. In the native membrane (called the purple membrane), bR assembles into trimers, which are arranged in a hexagonal lattice. bR has been extensively studied by optical spectroscopy techniques. Upon the absorption of light, photoisomerization from the all-*trans* conformation to the 13-*cis* conformation of the retinal chromophore takes place. This isomerization induces proton transfer from the Schiff base to Asp85, which triggers a cascade of changes in the bR structure. A series of intermediates designated as J–O are defined, among which M (M410), which has an absorption peak at 410 nm and the longest lifetime, is the only intermediate containing a deprotonated Schiff base [88]. In contrast to the spectroscopic characterization of bR during the photocycle, the overall dynamic structural change in bR upon photoactivation has long been elusive despite the establishment of its detailed static structure in the unphotolyzed state by X-ray crystallography and electron microscopy [91-93]. Thus, bR appears to be an ideal target for demonstrating the power of HS-AFM.

However, the photocycle of the wild type bR at neutral pH proceeds very fast (~10 ms). To slow down the photocycle, we used the D96N bR mutant that has a longer photocycle (~10 s at pH 7) but still retains the ability of proton pumping [94]. Native purple membranes containing D96N bR were directly placed on a bare mica surface. Figure 4 shows successive images of the D96N mutant at the cytoplasmic surface captured at 1 fps [10]. Upon illumination with green light (532 nm, 0.5 μW), bR markedly changed its structure (compare the images at 1 and 2 s) and returned to the ground state within a few seconds when light was discontinued. This structural change was specifically induced by green light and not by blue or red light, which is consistent with the fact that bR in the ground state effectively absorbs green light. The centers of mass of all activated bR monomers moved outwards by 0.7–0.8 nm

from the center of the respective trimers and rotated counterclockwise by 7–8° around the center of the respective trimers. The movement visualized here is ascribed to the displacement of the E–F loop, which was derived by the comparison with the atomic model of the α-helical cytoplasmic ends in the unphotolyzed state [90]. Note that the overall position of each bR molecule does not change because of indiscernible alterations at the extracellular surface. The photoactivated state observed by high-speed AFM was attributed to the spectroscopically identified M_N intermediate [11,95], which exhibits outward tilt of helix F similar to that in the N state of the wild type [96], while the Schiff-base is still deprotonated like the precedent M state because of the absence of the proton donor residue (D96) for the Schiff base. Thus, the photo-induced structural change in bR, which has long been studied but remained elusive, is now clearly revealed by its direct visualization.

As a result of the outward displacement, nearest-neighbor bR monomers (one set is shown with a light-blue circle in the image at 1 s in Fig. 4), each belonging to a different adjacent trimer (shown with three white circles), appear to transiently assemble (as indicated with a light-blue circle in the image at 2 s). Here, we use a new designation, ‘‘trefoil’’, for a triad of nearest-neighbor monomers belonging to different trimers to distinguish it from the original trimer. To investigate the possible effect of the bR-bR interaction within a trefoil on the photocycle, bR was illuminated with green light of different intensities (0.007–0.5 μW). Under weak illumination, only one monomer in each trefoil was activated in most cases. When only one monomer was activated in a trefoil, it decayed with a time constant of 7.3 ± 0.58 s. In contrast, under stronger illumination, two or three monomers within a trefoil tended to be activated together. Interestingly, the decay of each monomer markedly depended on the order of its activation. The monomer that was activated most recently among the activated monomers in a trefoil decayed with a shorter time constant of 2.0 ± 0.16 s. On the other hand, the decay kinetics of the monomers activated earlier did not follow a single exponential curve, and the average decay time lengthened to ~13 s. Thus, the bR-bR interaction within a trefoil under illumination engenders both positive and negative cooperative effects in the decay kinetics as the initial bR recovers.

Unlike previous expectations [97,98], these cooperativities do not occur within a trimer but within a trefoil. This finding was made possible by closely looking at individual bR molecules at a high spatial resolution in real space and real time. It is difficult to imagine how these cooperativities could have been found using techniques other than HS-AFM.

7. Future prospects of HS-AFM studies on molecular machines

7.1. Dynamic imaging of isolated biomolecular systems

Even for biomolecular systems that have already been studied in detail by other approaches, HS-AFM allows us to carry out more detailed inquiries or answer questions that have been difficult or impossible to address by other methods. Thus, HS-AFM provides the opportunity

to make unexpected new findings. This is indeed exemplified by our studies on M5-HMM, F_1-ATPase, and bR. Importantly, the HS-AFM instrument we have developed is now commercially available from the Research Institute of Biomolecule Metrology, Inc. (Tsukuba, Japan). Small cantilevers made of silicon nitride (9–10 μm long, 2 μm wide, and 130 nm thick; BL-AC10DS, Olympus, Tokyo) with f_c = 1.5 MHz in air and 0.6 MHz in water, k_c = 0.1 N/m, and quality factor Q ~2 in water are already commercially available. Smaller cantilevers are also being commercialized by NanoWorld. Therefore, it is expected that the expanded exploration by dynamic HS-AFM imaging will be carried out for a wide range of biomolecular systems in the near future. Thus, a comprehensive and deeper understanding of how biological molecular machines operate is expected to be attained and accelerated.

However, note that the successful visualization of dynamic events in biomolecular systems often requires much more defined conditions for the substrate surface than those in static AFM imaging. The substrate surface must have an appropriate affinity for the molecules. To observe dynamic interactions between different species of molecules, the selective attachment of one species of molecules to a surface is required. Otherwise, there is no chance to observe their interaction. Moreover, the sample on a surface can only be viewed from the direction perpendicular to the surface. Therefore, to observe the characteristic figure of molecules, they sometimes have to be placed in a particular orientation, as in the case of the observation of M5-HMM molecules walking on an actin filament [9]. For the selective attachment of one species of molecules, the following flat surfaces have thus far been characterized and used: (i) mica-supported phospholipid bilayers containing functional lipids [9,18] and (ii) two-dimensional crystals of streptavidin formed on biotin-containing lipid bilayers [18,27,99]. To observe dynamic DNA-protein interactions, DNA origami tiles [35,38] seem useful when they are placed on a surface resistant to nonspecific binding such as a phospholipid bilayer surface. Various substrate surfaces are expected to be developed along with the expansion of HS-AFM imaging studies.

7.2. Dynamic *insitu* imaging of molecules on higher-order structures

The fast scanners that we have developed are optimized for the high-speed imaging of isolated biomolecules; their resonant frequencies are very high but the scan range is limited to 1 μm, 4 μm, and 1 μm in the x-, y-, and z-directions (at 100 V), respectively. Therefore, large samples such as live bacterial and mammalian cells have not been able to be imaged by HS-AFM until recently. To overcome this limitation, we have recently developed a wide-area scanner that can be displaced by up to 43 μm in the x- and y-directions and 2.5–4 μm in the z-direction. The resonant frequency of its x- and y-scanners is low (~1.6 kHz) but can be increased to ~10 kHz by an inverse compensation-based active damping technique [7]. Using this scanner and another medium-range scanner, whole live bacterial cells have recently been visualized. After taking an image of an entire magnetic bacterial cell, part of its outer surface was imaged fast, enabling the visualization of densely packed but rapidly diffusing porin

molecules [100]. This capacity will provide new opportunities for the *insitu* dynamic imaging of molecular machines on higher-order structures such as live mitochodoria, nuclei, and neuronal spines.

Acknowledgements

I would like to thank Takayuki Uchihashi, Noriyuki Kodera, Daisuke Yamamoto, Hayato Yamashita, Mikihiro Shibata, Ryota Iino, Hiroyuki Noji, and Hideki Kandori for collaborations and discussions on the topics described in this review. This work was supported by a Grant-in-Aid for Basic Research S (20221006 and 24227005) from the Ministry of Education, Culture, Sports, Science and Technology of Japan, by the Knowledge Cluster Initiative Project, and by the CREST project from the Japan Science and Technology Agency.

Legends for Figures

Fig. 1. Schematic of tapping-mode AFM setup (see text).

Fig. 2. Walking M5-HMM captured by HS-AFM. (A) Successive AFM images showing processive movement of M5-HMM in 1 μM ATP. Frame rate, 7 fps. (B) Schematic of two-headed bound M5-HMM. (C) Successive AFM images showing hand-over-hand movement in 1 μM ATP. Frame rate, 7 fps. The swinging lever is highlighted with a thin white line. (D) Schematic explanation of the images in C. The "+" marks indicate the plus ends of actin filaments. (E) A model of mechanochemical coupling in actin-myosin interaction proposed on the basis of the swinging lever-arm hypothesis for muscle contraction.

Fig. 3. AFM images of $\alpha_3\beta_3$ subcomplex at C-terminal surface. (A) Schematic of F_1-ATPase. (B) Averaged AFM image obtained under nucleotide-free condition. (C) C-terminal surface of crystal structure of nucleotide-free $\alpha_3\beta_3$ subcomplex. (D) Simulated AFM image of (C). (E) Averaged AFM image obtained in 1 mM AMP-PNP. (F) C-terminal surface of crystal structure of $\alpha_3\beta_3$ subcomplex obtained in ATP. (G) Simulated AFM image of (F). (H) Successive images of C-terminal surface of $\alpha_3\beta_3$ subcomplex in 2 μM ATP, captured by HS-AFM at 12.5 fps. The highest pixel position in each image is marked with a red circle.

Fig. 4. Successive images of the cytoplasmic surface of D96N bR under dark and illuminated conditions, captured by HS-AFM at 1 fps. The green bars at 2 and 3 s indicate the illumination of 532 nm green light with an intensity of 0.5 μW. A bR trimer is highlighted with a white triangle in the image at 0 s. In the image at 1 s, three adjacent trimers are

encircled with white circles, while a trefoil comprised of three nearest-neighbor monomers, each belonging to one of the encircled trimers, is indicated with a light-blue circle. Compare the structures of the same trefoil at 2 and 3 s.

References

[1] Joo, C., Balci, H., Ishitsuka, Y., Buranachai, C. and Ha, T. (2008) Advances in single-molecule fluorescence methods for molecular biology. Annu. Rev. Biochem. 77, 51–76.

[2] Huang, B., Bates, M. and Zhuang, X. (2009) Super-resolution fluorescence microscopy. Annu. Rev. Biochem. 78, 993–1016.

[3] Moffitt, J. R., Chemla, Y. R., Smith, S. B. and Bustamante, C. (2008) Recent advances in optical tweezers. Annu. Rev. Biochem. 77, 205–228.

[4] Neuman, K. C. and Block, S. M. (2004) Optical trapping. Rev. Sci. Instrum. 75, 2787–2809.

[5] Binnig, G., Quate, C. F. and Gerber, Ch. (1986) Atomic force microscope. Phys. Rev. Lett. 56, 930–933.

[6] Ando, T., Kodera, N., Takai, E., Maruyama, D., Saito, K. and Toda, A. (2001) A high-speed atomic force microscope for studying biological macromolecules. Proc. Natl. Acad. Sci. USA 98, 12468–12472.

[7] Ando, T., Uchihashi, T. and Fukuma, T. (2008) High-speed atomic force microscopy for nano-visualization of dynamic biomolecular processes. Prog. Surf. Sci. 83, 337–437.

[8] Ando, T. (2012) High-speed atomic force microscopy coming of age. Nanotechnology 23, 062001 (27 pp).

[9] Kodera, N., Yamamoto, D., Ishikawa, R. and Ando, T. (2010) Video imaging of walking myosin V by high-speed atomic force microscopy. Nature 468, 72–76.

[10] Shibata, M., Yamashita, H., Uchihashi, T., Kandori, H. and Ando, T. (2010) High-speed atomic force microscopy shows dynamic molecular processes in photo-activated bacteriorhodopsin. Nat. Nanotechnol. 5, 208–212 (2010).

[11] Shibata, M., Uchihashi, T., Yamashita, H., Kandori, H. and Ando, T. (2011) Structural changes in bacteriorhodopsin in response to alternate illumination observed by high-speed atomic force microscopy. Angew. Chem. Int. Ed. 50, 4410–4413.

[12] Uchihashi, T., Iino, R., Ando, T. and Noji, H. (2011) High-speed atomic force microscopy reveals rotary catalysis of rotorless F_1-ATPase. Science 333, 755–758.

[13] Zhong, Q., Inniss, D., Kjoller, K. and Elings, V. B. (1993) Fractured polymer/silica fiber surface studied by tapping mode atomic force microscopy. Surf. Sci. 290, L688–L692.

[14] Walters, D. A., Cleveland, J. P., Thomson, N. H., Hansma, P. K., Wendman, M. A., Gurley, G. and Elings, V. (1996) Short cantilevers for atomic force microscopy. Rev. Sci. Instrum. 67, 3583–3590.

[15] Kitazawa, M., Shiotani, K. and Toda, A. (2003) Batch fabrication of sharpened silicon nitride tips. Jpn. J. Appl. Phys. 42, 4844–4847.

[16] Kodera, N., Yamashita, H. and Ando, T. (2005) Active damping of the scanner for high-speed atomic force microscopy. Rev. Sci. Instrum. 76, 053708 (5 pp).

[17] Kodera, N., Sakashita, M. and Ando, T. (2006) Dynamic proportional-integral-differential controller for high-speed atomic force microscopy. Rev. Sci. Instrum. 77, 083704 (7 pp).

[18] Uchihashi, T., Kodera, N. and Ando, T. (2012) Guide to video recording of structure dynamics and dynamic processes of proteins by high-speed atomic force microscopy. Nat. Protoc. 7, 1193–1206.

[19] Shinozaki, Y., Sumitomo, K., Tsuda, M., Koizumu, S., Inoue, K. and Torimitsu, K. (2009) Direct observation of ATP-induced conformational changes in single $P2X_4$ receptors. PLoS Biol. 7, e1000103 (12 pp).

[20] Yamamoto, D., Uchihashi, T., Kodera, N. and Ando, T. (2008) Anisotropic diffusion of point defects in two-dimensional crystal of streptavidin observed by high-speed atomic force microscopy. Nanotechnology 19, 384009 (9 pp).

[21] Miyagi, A., Tsunaka, Y., Uchihashi, T., Mayanagi, K., Hirose, S., Morikawa, K. and Ando, T. (2008) Visualization of intrinsically disordered regions of proteins by high-speed atomic force microscopy. Chem. Phys. Chem. 9, 1859–1866.

[22] Casuso, I., Khao, J., Paul-Gilloteaux, P., Husain, M., Duneau, J.-P., Stahlberg, H., Sturgis, J. N. and Scheuring, S. (2012) Characterization of the motion of membrane proteins using high-speed atomic force microscopy. Nat. Nanotechnol. 7, 525–529.

[23] Sanchez, H., Suzuki, Y., Yokokawa, M., Takeyasu, K. and Wyman, C. (2011) Protein-DNA interactions in high speed AFM: single molecule diffusion analysis of human RAD54. Integr. Biol. 3, 1127–1134.

[24] Casuso, I., Sens, P., Rico, F. and Scheuring, S. (2010) Experimental evidence for membrane-mediated protein-protein interaction. Biophys. J. 99, L47–L49.

[25] Casuso, I., Kodera, N., Le Grimellec, Ch., Ando, T. and Scheuring, S. (2009) High-resolution high-speed contact mode atomic force microscopy movies of purple membrane. Biophys. J. 97, 1354–1361.

[26] Yamashita, H., Voïtchovsky, K., Uchihashi, T., Antoranz Contera, S., Ryan, J. F. and Ando, T. (2009) Dynamics of bacteriorhodopsin 2D crystal observed by high-speed atomic force microscopy. J. Struct. Biol. 167, 153–158.

[27] Yamamoto, D., Nagura, N., Omote, S., Taniguchi, M. and Ando, T. (2009) Streptavidin 2D crystal substrates for visualizing biomolecular processes by atomic force microscopy. Biophys. J. **97** 2358–2367.

[28] Yokokawa, M., Wada, C., Ando, T., Sakai, N., Yagi, A., Yoshimura, S. H. and Takeyasu, K. (2006) Fast-scanning atomic force microscopy reveals the ATP/ADP-dependent conformational chnages of GroEL. EMBO J. 25, 4567–4576.

[29] Milhiet, P.-E., Yamamoto, D., Berthoumieu, O., Dosset, P., Le Grimellec, Ch., Verdier, J.-M., Marchal, S. and Ando, T. (2010) Deciphering the structure, growth and assembly of amyloid-like fibrils using high-speed atomic force microscopy. PLoS ONE 5, e13240 (8 pp).

[30] Giocondi, M.-C., Yamamoto, D., Lesniewska, E., Milhiet, P.-E., Ando, T. and Le Grimellec, Ch. (2010) Surface topography of membrane domains. Biochim. Biophys. Acta. Biomembranes 1798, 703–718.

[31] Igarashi, K., Koivula, A., Wada, M., Kimura, S., Penttilä, M. and Samejima, M. (2009) High speed atomic force microscopy visualizes processive movement of *Trichoderma reesei* cellobiohydrolase I on crystalline cellulose. J. Biol. Chem. 284, 36186–36190.

[32] Igarashi, K., Uchihashi, T., Koivula, A., Wada, M., Kimura, S., Okamoto, T., Penttilä, M., Ando, T. and Samejima, M. (2011) Traffic jams reduce hydrolytic efficiency of cellulase on cellulose surface. Science 333, 1279–1282.

[33] Gilmore, J. L., Suzuki, Y., Tamulaitis, G., Siksnys, V., Takeyasu, K. and Lyubchenko, Y. L. (2009) Single-molecule dynamics of the DNA−*Eco*RII protein complexes revealed with high-speed atomic force microscopy. Biochemistry 48, 10492–10498.

[34] Suzuki, Y., Gilmore, J. L., Yoshimura, S. H., Henderson, R. M., Lyubchenko, Y. L. and Takeyasu, K. (2011) Visual analysis of concerted cleavage by type IIF restriction enzyme SfiI in subsecond time region. Biophys. J. 101, 2992–2998.

[35] Sannohe, Y., Endo, M., Katsuda, Y., Hidaka, K. and Sugiyama, H. (2010) Visualization of dynamic conformational switching of the G-quadruplex in a DNA nanostructure. J. Am. Chem. Soc. 132, 16311–16313.

[36] Wickham, F. J. S., Endo, M., Katsuda, Y., Hidaka, K., Bath, J., Sugiyama, H. and Turberfield, A. J. (2011) Direct observation of stepwise movement of a synthetic molecular transporter. Nat. Nanotechnol. 6, 166–169.

[37] Endo, M., Hidaka, K. and Sugiyama, H. (2011) Direct AFM observation of an opening event of a DNA cuboid constructed via a prism structure. Org. Biomol. Chem. 9, 2075–2077.

[38] Endo, M., Katsuda, Y., Hidaka, K. and Sugiyama, H. (2010) Regulation of DNA methylation using different tensions of double strands constructed in a defined DNA nanostructure. J. Am. Chem. Soc. 132, 1592–1597.

[39] Tanaka, F., Mochizuki, T., Liang, X., Asanuma, H., Tanaka, S., Suzuki, K., Kitamura, S., Nishikawa, A., Ui-Tei, K. and Hagiya, M. (2010) Robust and photocontrollable DNA capsules using azobenzenes. Nano Lett. 10, 3560–3565.

[40] Phillips, R., Ursell, T., Wiggins, P. and Sens, P. (2009) Emerging roles for lipids in shaping membrane-protein function. Nature 459, 379–385.

[41] Sellers, J. R. & Weisman, L. S. (2008) Myosin V. In Myosins: A Superfamily of Molecular Motors. Proteins and Cell Regulation Vol. 7. (Coluccio, L., ed), pp. 289–324. Springer, Netherlands.

[42] Mehta, A. D., Rock, R. S., Rief, M., Spudich, J. A., Mooseker, M. S. and Cheney, R. E. (1999) Myosin–V is a processive actin-based motor. Nature 400, 590–593.

[43] Sakamoto, T., Amitani, I., Yokota, E. and Ando, T. (2000) Direct observation of processive movement by individual myosin V molecules. Biochem. Biophys. Res. Commun. 272, 586–590.

[44] Yildiz, A., Forkey, J. N., McKinney, S. A., Ha, T., Goldman, Y. E. and Selvin, P. R. (2003) Myosin V walks hand-over-hand: Single fluorophore imaging with 1.5-nm localization. Science 300, 2061–2065.

[45] Forkey, J. N., Quinlan, M. E., Shaw, M. A., Corrier, J. E. T. and Goldman, Y. E. (2003) Three-dimensional structural dynamics of myosin V by single-molecule fluorescence polarization. Nature 422, 399–404.

[46] Warshaw, D. M., Kennedy, G. G., Work, S. S., Krementsova, E. B., Beck, S. and Trybus, K. M. (2005) Differential labeling of myosin V heads with quantum dots allows direct visualization of hand-over-hand processivity. Biophys. J. 88, L30–L32.

[47] Sakamoto, T., Webb, M. R., Forgacs, E., White, H. D. and Sellers, J. R. (2008) Direct observation of the mechanochemical coupling in myosin Va during processive movement. Nature 455, 128–132.

[48] Walker, M. L., Burgess, S. A., Sellers, J. R., Wang, F., Hammer III, J. A., Trinick, J. and Knight, P. J. (2000) Two-headed binding of a processive myosin to F-actin. Nature 405, 804–807.

[49] Burgess, S. Walker, M., Wang, F., Sellers, J. R., White, H. D., Knight, P. J. (2002) The prepower stroke conformation of myosin V. J. Cell Biol. 159, 983–991.

[50] Hua, W., Chung, J. and Gelles, J. (2002) Distinguishing inchworm and hand-over-hand processive kinesin movement by neck rotation measurements. Science 295, 844–848.

[51] Okada, T., Tanaka, H., Hikikoshi Iwane, A., Kitamura, K., Ikebe, M. and Yanagida, T. (2007) The diffusive search mechanism of processive myosin class-V motor involves directional steps along actin subunits. Biochem. Biophys. Res. Commun. 354, 379–384.

[52] Huxley, H. E. (1969) The mechanism of muscular contraction. Science 164, 1356–1366.

[53] Wang, F., Chen, L., Arcucci, O., Harvey, E. V., Bowers, B., Xu, Y., Hammer III, J. A. and Sellers, J. R. (2000) Effect of ADP and ionic strength on the kinetic and motile properties of recombinant mouse myosin V. J. Biol. Chem. 275, 4329–4335.

[54] Geeves, M. A. and Holmes, K. C. (1999) Structural mechanism of muscle contraction. Annu. Rev. Biochem. 68, 687–728.

[55] Goldman, Y. E. (1987) Kinetics of the actomyosin ATPase in muscle fibers. Annu. Rev. Physiol. 49, 637–654.

[56] De La Cruz, E. M., Wells, A. L., Rosenfeld, S. S., Ostap, E. M. and Sweeney, H. L. (1999) The kinetic mechanism of myosin V. Proc. Natl. Acad. Sci. USA 96, 13726–13731.

[57] Rosenfeld, S. S. and Sweeney, H. L. (2004) A model of myosin V processivity. J. Biol. Chem. 279, 40100–40111.

[58] Veigel, C., Schmitz, S., Wang, F. and Sellers, J. R. (2005) Load-dependent kinetics of myosin-V can explain its high processivity. Nat. Cell Biol. 7, 861–869.

[59] Oguchi, Y., Mikhailenko, S. V., Ohki, T., A. Olivares, O., De La Cruz, E. M. and Ishiwata, S. (2008) Load-dependent ADP binding to myosins V and VI: Implications for subunit coordination and function. Proc. Natl. Acad. Sci. USA 105, 7714–7719.

[60] Purcell, T. J., Sweeney, H. L. and Spudich, J. A. (2005) A force-dependent state controls the coordination of processive myosin V. Proc. Natl. Acad. Sci. USA 102, 13873–13878.

[61] Forgacs, E., Cartwright, S., Sakamoto, T., Sellers, J. R. and Corrie, J. E. T., Webb, M. R. and White, H. D. (2008) Kinetics of ADP dissociation from the trail and lead heads of actomyosin V following the power stroke. J. Biol. Chem. 283, 766–773.

[62] Fisher, A. J., Smith, C. A., Thoden, J. B., Smith, R., Sutoh, K., Holden, H. M. and Rayment, I. (1995) X-ray structures of the myosin motor domain of *Dictyostelium discoideum* complexed with MgADP-BeF_x, and MgADP-AlF_4^-. Biochemistry 34, 8960–8972.

[63] Smith, C. A. and Rayment, I. (1996) X-ray structure of the magnesium(II)·ADP ·vanadate complex of the *Dictyostelium discoideum* myosin motor domain to 1.9 Å resolution. Biochemistry 35, 5404–5417.

[64] Dominguez, R., Freyzon, Y., Trybus, K. M. and Cohen, C. (1998) Crystal structure of a vertebrate smooth muscle myosin motor domain and its complex with the essential light chain: Visualization of the pre–power stroke state. Cell 94, 559–571.

[65] Houdusse, A., Szent-Györgyi, A. G. and Cohen, C. (2000) Three conformational states of scallop myosin S1. Proc. Natl. Acad. Sci. USA 97, 11238–11243.

[66] Coureux, P.-D., Sweeney, H. L. and Houdusse, A. (2004) Three myosin V structures delineate essential features of chemo-mechanical transduction. EMBO J. 23, 4527–4537.

[67] Volkmann, N., Liu, H. J., Hazelwood, L., Krementsova, E. B., Lowey, S., Trybus, K. M. and Hanein, D. (2005) The structural basis of myosin V processive movement as revealed by electron cryomicroscopy. Mol. Cell 19, 595–605.

[68] Thomas, D. D., Kast, D. and Korman V. L. (2009) Site-directed spectroscopic probes of actomyosin structural dynamics. Annu. Rev. Biophys. 38, 347–369.

[69] Baker, J. E., Brust-Mascher, I., Ramachandra, S., LaConte, L. E. and Thomas, D. D. (1998) A large and distinct rotation of the myosin light chain domain occurs upon muscle contraction. Proc. Natl. Acad. Sci. USA 95, 2944–2949.

[70] Nakajima, H., Kunioka, Y., Nakano, K., Shimizu, K., Seto, M. and Ando, T. (1997) Scanning force microscopy of the interaction events between a single molecule of heavy meromyosin and actin. Biochem. Biophys. Res. Commun. 234, 178–182.

[71] Hinterdorfer, P., Baumgartner,W., Gruber, H. J., Schilcher, K. and Schindler, H. (1996) Detection and localization of individual antibody-antigen recognition events by atomic force microscopy. Proc. Natl. Acad. Sci. USA 93, 3477–3481.

[72] Yuan, C., Chen, A., Kolb, P. and Moy, V. T. (2000) Energy landscape of streptavidin-biotin complexes measured by atomic force microscopy. Biochemistry 39, 10219–10223.

[73] Miyata, H., Yasuda, R. and Kinosita, K. Jr. (1996) Strength and lifetime of the bond between actin and skeletal muscle α-actinin studied with an optical trapping technique. Biochim. Biophys. Acta 1290, 83–88

[74] Milligan, R. A. (1996) Protein-protein interactions in the rigor actomyosin complex. Proc. Natl. Acad. Sci. USA 93, 21–26.

[75] Kabsch, W., Mannherz, H. G., Suck, D., Pai, E. F. and Holmes, K. C. (1990) Atomic structure of the actin: Dnase I complex. Nature 347, 37–44.

[76] Howard, J. (2001) Mechanics of Motor Proteins and the Cytoskeleton. Signauer Associates, Inc, Massachusetts.

[77] Gresser, M. J., Myers, J. A. and Boyer, P. D. (1982) Catalytic site cooperativity of beef heart mitochondrial F_1 adenosine triphosphatase. Correlations of initial velocity, bound intermediate, and oxygen exchange measurements with an alternating three-site model. *J. Biol. Chem*. 257, 12030–12038.

[78] Noji, H., Yasuda, R., Yoshida, M. and Kinosita, K. Jr. (1997) Direct observation of the rotation of F_1-ATPase. Nature 386, 299–302.

[79] Yasuda, R., Noji, H., Kinosita, K. Jr. and Yoshida, M. (1998) F_1-ATPase is a highly efficient molecular motor that rotates with discrete 120° steps. Cell 93, 1117–1124.

[80] Abrahams, J. P., Leslie, A. G., Lutter, R. and Walker, J. E. (1994) Structure at 2.8 Å resolution of F_1-ATPase from bovine heart mitochondria. Nature 370, 621–628.

[81] Wang, H. and Oster, G. (1998) Energy transduction in the F_1 motor of ATP synthase. Nature 396, 279–282.

[82] Itoh, H., Takahashi, A., Adachi, K., Noji, H., Yasuda, R., Yoshida, K. and Kinoshita, K. Jr. (2004) Mechanically driven ATP synthesis by F_1-ATPase. Nature 427, 465–468.

[83] Rondelez, Y., Tresset, G., Nakashima, T., Kato-Yamada, Y., Fujita, H., Takeuchi, S. and Noji, H. (2005) Highly coupled ATP synthesis by F1-ATPase single molecules. Nature 433, 773–777.

[84] Iko, Y., Tabata, K. V., Sakakihara, S., Nakashima, T. and Noji, H. (2009) Acceleration of the ATP-binding rate of F_1-ATPase by forcible forward rotation. FEBS Lett. 583, 3187–3191.

[85] Furuike, S., Hossain, M. D., Maki, Y., Adachi, K., Suzuki, T., Kohori, A., Itoh, H.,

Yoshida, M. and Kinoshita, K. Jr. (2008) Axle-less F_1-ATPase rotates in the correct direction. Science 319, 955–958.

[86] Shirakihara, Y., Leslie, A. G., Abrahams, J. P., Walker, J. E., Ueda, T., Sekimoto, Y., Kambara, M., Kagawa, Y. and Yoshida, M. (1997) The crystal structure of the nucleotide-free alpha 3 beta 3 subcomplex of F_1-ATPase from the thermophilic Bacillus PS3 is a symmetric trimer. Structure 5, 825–36.

[87] Haupts, U., Tittor, J. and Oesterhelt, D. (1999) Closing in on bacteriorhodopsin: Progress in understanding the molecule. Annu. Rev. Biophys. Biomol. Struct. 28, 367–399.

[88] Lanyi, J. K. (2004) Bacteriorhodopsin. Annu. Rev. Physiol. 66, 665–688.

[89] Kimura, Y., Vassylyev, D. G., Miyazawa, A., Kidera, A., Matsushima, M., Mitsuoka, K., Murata, K., Hirai, T. and Fujiyoshi, Y. (1997) Surface of bacteriorhodopsin revealed by high-resolution electron crystallography. Nature 389, 206–211.

[90] Luecke, H., Schobert, B., Richter, H. T., Cartailler, J. P. and Lanyi, J. K. (1999) Structure of bacteriorhodopsin at 1.55 Å resolution. J. Mol. Biol. 291, 899–911.

[91] Luecke, H., Schobert, B., Lanyi, J. K., Spudich, E. N. and Spudich, J. L. (2001) Crystal structure of sensory rhodopsin II at 2.4 Angstroms: Insights into color tuning and transducer interaction. Science 293, 1499–1503.

[92] Sass, H. J., Büldt, G., Gessenich, R., Hehn, D., Neff, D., Schlesinger, R., Berendzen, J. and Ormos, P. (2000) Structural alterations for proton translocation in the M state of wild-type bacteriorhodopsin. Nature 406, 649–653.

[93] Subramaniam, S. and Henderson, R. (2000) Molecular mechanism of vectorial proton translocation by bacteriorhodopsin. Nature 406, 653–657.

[94] Otto, H., Marti, T., Holz, M., Mogi, T., Lindau, M., Khorana, H. G. and Heyn, M. P. (1989) Aspartic acid-96 is the internal proton donor in the reprotonation of the Schiff base of bacteriorhodopsin. Proc. Natl. Acad. Sci. USA. 86, 9228–9232.

[95] Kamikubo, H., Kataoka, M., Varo, G., Oka, T., Tokunaga, F., Needleman, R. and Lanyi, J. K. (1996) Structure of the N intermediate of bacteriorhodopsin revealed by x-ray diffraction. Proc. Natl. Acad. Sci. USA 93, 1386-1390.

[96] Vonck, J. (1996) A three-dimensional difference map of the N intermediate in the bacteriorhodopsin photocycle: part of the F helix tilts in the M to N transition. Biochemistry 35, 5870-5878.

[97] Komrakov, A. Y. and Kaulen, A. D. (1995) M-decay in the bacteriorhodopsin photocycle: effect of cooperativity and pH. Biophy. Chem. 56, 113–119.

[98] Tokaji, Z. (1997) Dimeric-like kinetic cooperativity of the bacteriorhodopsin molecules in purple membranes. Biophys. J. 65, 1130–1134.

[99] Yamamoto, D., Uchihashi, T., Kodera, N., Yamashita, H., Nishikori, S., Ogura, T., Shibata, M. and Ando, T. (2010) High-speed atomic force microscopy techniques for observing dynamic biomolecular processes. Methods Enzymol. 475, 541–564.

[100] Yamashita, H., Taoka, A., Uchihashi, T., Asano, T., Ando, T. and Fukumori, Y. (2012) Single molecule imaging on living bacterial cell surface by high-speed AFM. J. Mol. Biol. 422, 300–309.

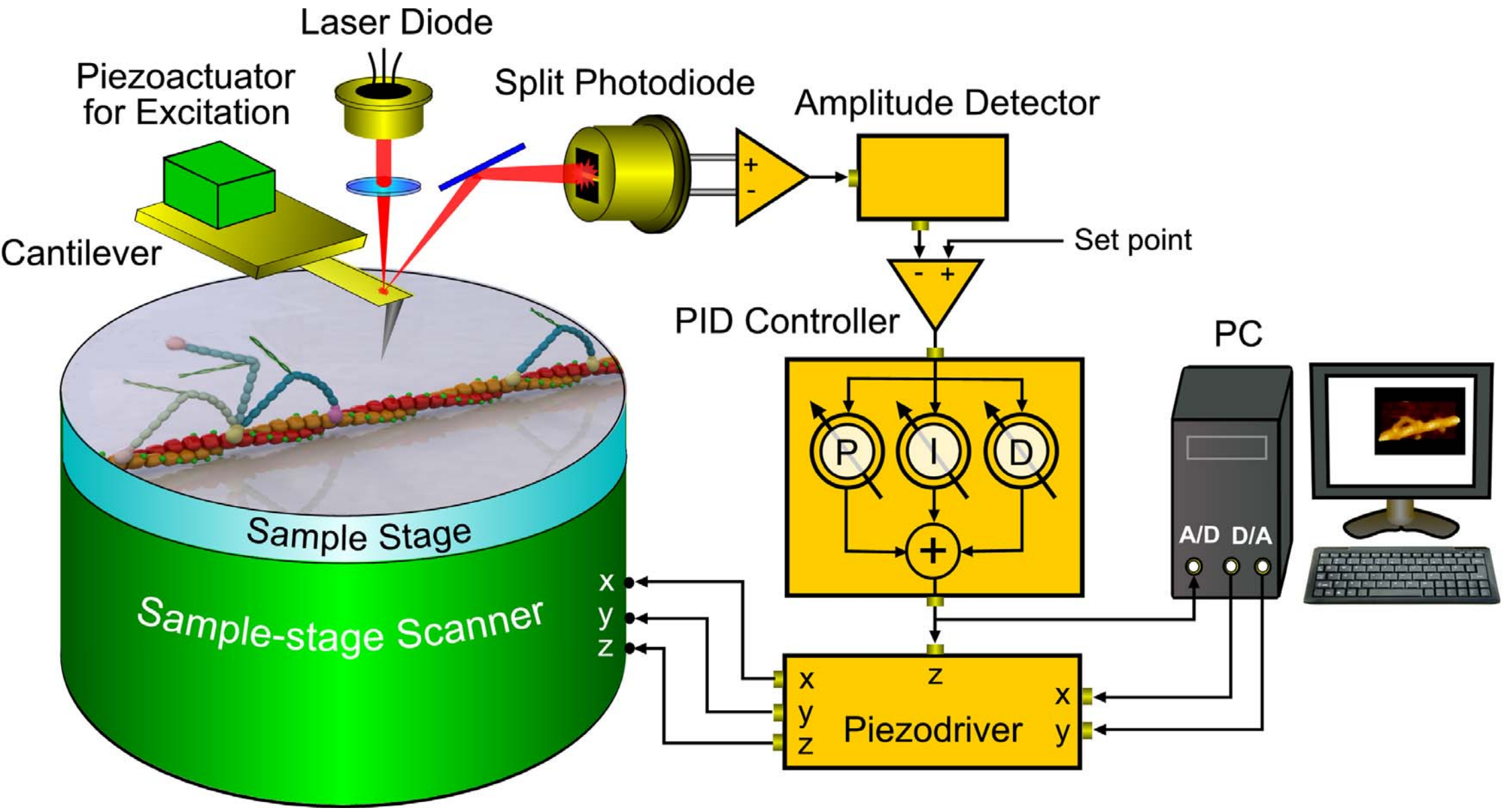
Laser Diode
Piezoactuator for Excitation
Split Photodiode
Amplitude Detector
Cantilever
Set point
PID Controller
PC
P
I
D
A/D
D/A
Sample Stage
Sample-stage Scanner
x
y
z
Piezodriver

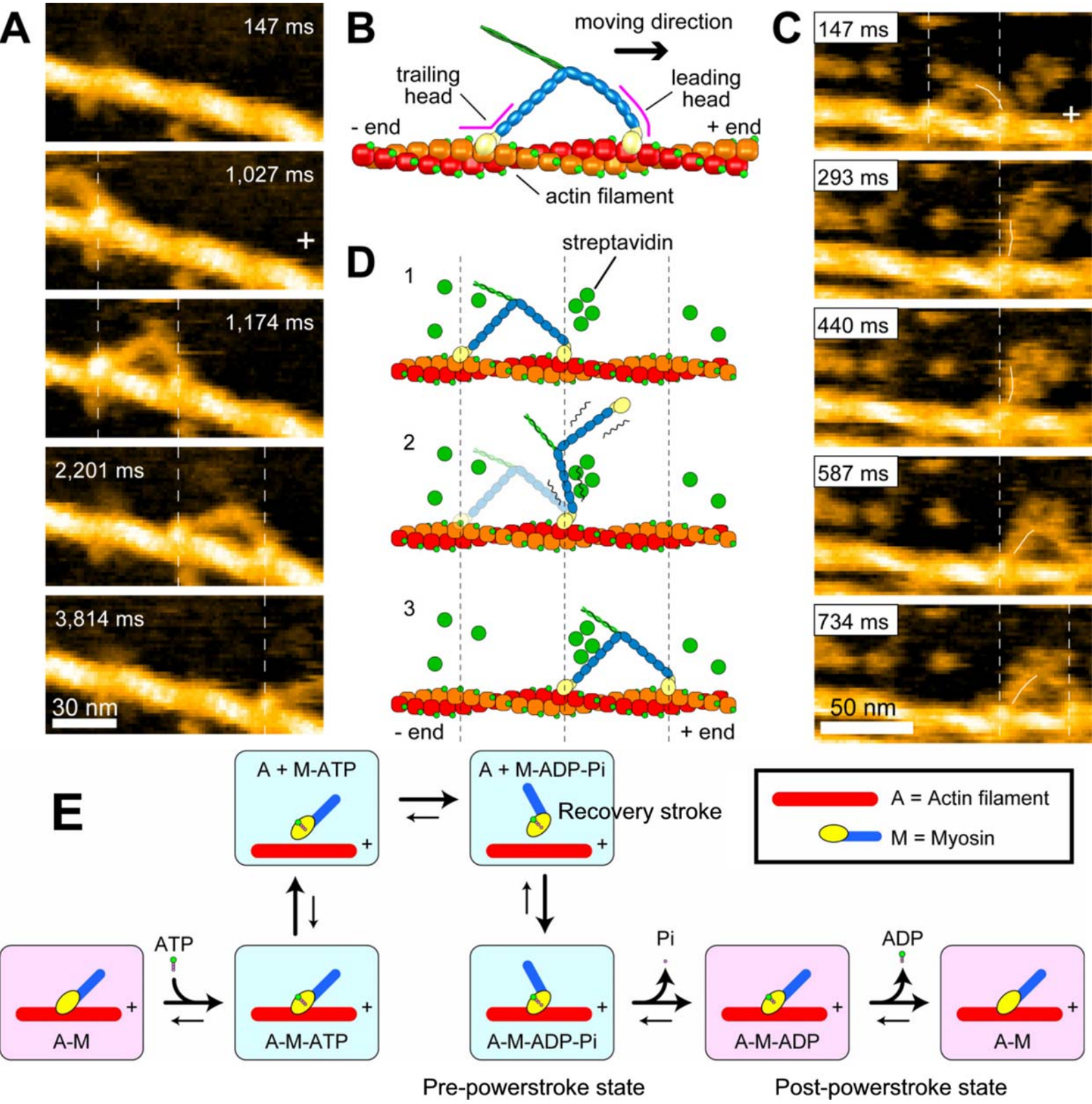
A
147 ms
1,027 ms
+
1,174 ms
2,201 ms
3,814 ms
30 nm
B
moving direction
trailing head
leading head
- end
+ end
actin filament
C
147 ms
+
293 ms
440 ms
587 ms
734 ms
50 nm
D
streptavidin
1
2
3
- end
+ end
E
A + M-ATP
A + M-ADP-Pi
Recovery stroke
A = Actin filament
M = Myosin
ATP
Pi
ADP
A-M
A-M-ATP
A-M-ADP-Pi
A-M-ADP
A-M
Pre-powerstroke state
Post-powerstroke state

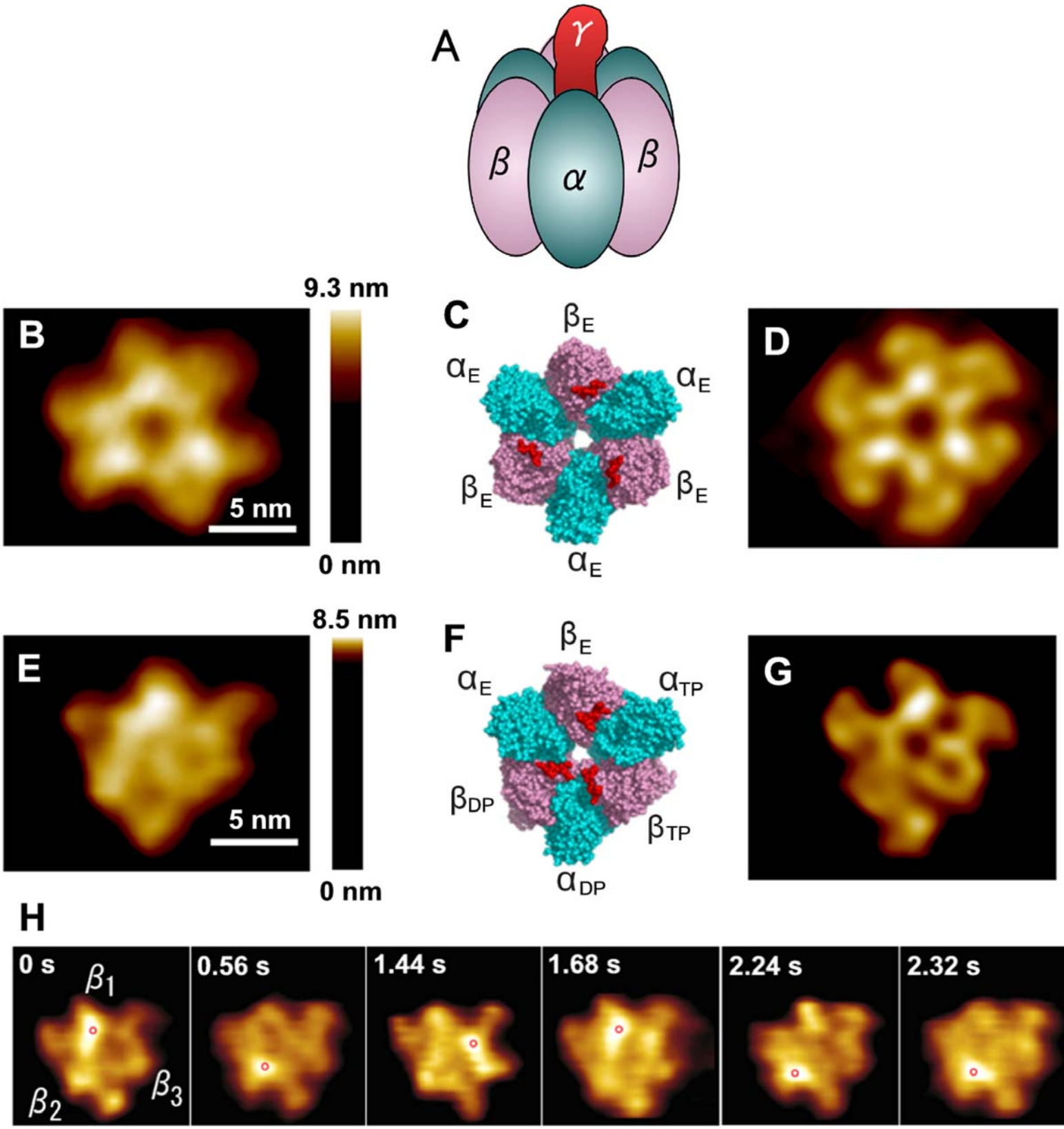
A
γ
β
α
β
B
9.3 nm
5 nm
0 nm
C
βE
αE
αE
βE
βE
αE
D
E
8.5 nm
5 nm
0 nm
F
βE
αE
αTP
βDP
βTP
αDP
G
H
0 s
β1
β2
β3
0.56 s
1.44 s
1.68 s
2.24 s
2.32 s

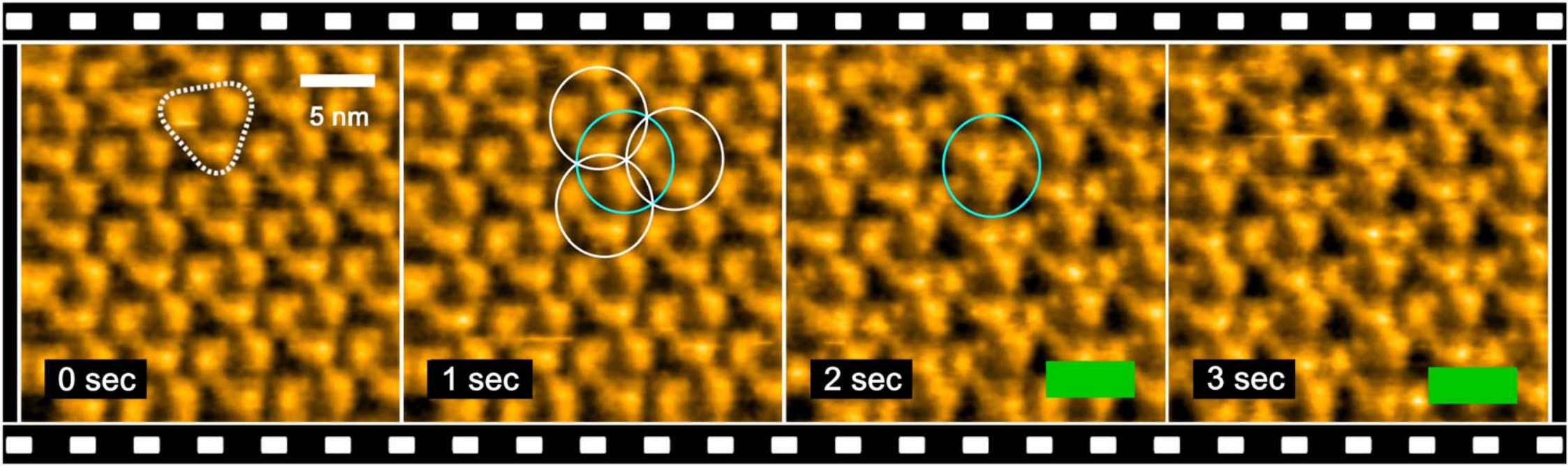
5 nm
0 sec
1 sec
2 sec
3 sec